Algorithms for Korringa-Kohn-Rostoker electronic structure calculations in any Bravais lattice

E. Bruno and B. Ginatempo
Dipartimento di Fisica and Unità INFM, Università di Messina Salita Sperone 31, 98166 Messina, Italy
(Received 28 August 1996; revised manuscript received 27 January 1997)

We present some algorithms for improvements of band theory calculations based on the Korringa-Kohn-Rostoker method and on the coherent potential approximation, in the cases of ordered metals and random alloys. The purpose of our work was to develop a code flexible enough to deal on equal footing with any lattice geometry. The algorithms proposed are designed to achieve an arbitrary accuracy and to minimize the required computational efforts. In particular, we describe (i) an efficient and accurate method for the calculation of the KKR structure constants, and (ii) an adaptive method for the Brillouin zone integration. These algorithms have been tested for a free-electron Green's function and by explicit calculations for a number of systems and, when possible, discussed in comparison with other methods. *Ab initio* calculations for hexagonal close packed and face centered cubic Ti and for $Cu_{0.75}$-$Pt_{0.25}$ random alloys are presented. [S0163-1829(97)10716-0]

I. INTRODUCTION

The Korringa-Kohn-Rostoker (KKR) method,[1,2] when compared with other band theory methods, has the advantage of dealing with small size matrices owing to the fast convergence of scattering operators in the angular momentum space. A further advantage is that of dealing with Green's functions. This is particularly valuable in the case of random metallic alloys, where this feature allows us to carry out with relative ease the ensemble configuration averages, necessary in order to evaluate the alloy physical observables. These averages can be computed by various approximations, among which the coherent potential approximation (CPA) (Ref. 3) has been one of the most successful and reliable approaches.[4] Moreover, the numerical implementation of the KKR-CPA is efficiently parallelizable,[5] either by supercomputers or workstations clusters. There are, of course, a few inconveniences.

At first, the so-called KKR structure constants,[6,7] the empty lattice propagators, depend on the energy, and the existing algorithms require their calculation to be carried out for each energy at many reciprocal space points. This is usually accomplished by applying the famous Ewald's Θ transform[8] and is computationally expensive. Another shortcoming is that the KKR matrix has a pole structure and that makes its Brillouin zone (BZ) integration difficult. This usually requires a number of $\vec{k}$ points larger than for other band theory methods.

The most popular and efficient way to reduce the numerical effort for the structure constants calculation is due to Stocks *et al.*,[9,10] who separated the structure constants in a regular and an irregular part, by isolating the free-electron poles. The regular part turns out to be a smooth function of the energy E and the momentum $\vec{k}$, and thus it can be interpolated by, for instance, Tchebyschev polynomials. Remarkably, for cubic lattices and using appropriate units, the polynomial coefficients do not depend on the lattice parameters. As a consequence, a great flexibility in designing BZ integration algorithms has been achieved[9–11] allowing for the practical feasibility of KKR-CPA calculations in the past two decades.

The above fitting technique has the practical inconvenience of requiring as many different sets of coefficients as the nonequivalent translations between pairs of scatterers in the unit cell. Furthermore, for noncubic systems, these coefficients depend on all but one of the lattice parameters. Namely, for tetragonal lattices, either different sets of coefficients for each value of c/a would be required, or a further fit in the c/a space would be necessary. This circumstance, among others, has made it difficult to implement KKR-CPA calculations for complex lattice structures such as, for instance, cuprates.

A different summation scheme for the KKR structure constants, which does not require any interpolation, was proposed by Giannozzi *et al.*[12] It does not present any problem when dealing with complicated lattice geometries, however its practical utility is restricted to algorithms employing fixed reciprocal space meshes for the BZ integration.

Most of band-structure methods deal with eigenvalues and eigenvectors rather than Green's functions. For these methods, uniform BZ integration grids, as in the tetrahedron or the special points methods,[13,14] are accurate and widely employed. These grids, unfortunately, are not efficient for KKR calculations, where a dense mesh of points is necessary in a neighborhood of the poles, while few points are able to sample the remainder of the integration domain.

Various BZ integration techniques have been implemented specifically for the KKR method. The use of the tetrahedron method within the KKR framework needs some manipulations of the integrands. Zeller and others,[15] in order to smooth out the integrands in proximity to the free-electron poles, designed an algorithm based on a supermatrix partitioning. This method, however, cannot isolate the KKR matrix poles due to resonant scattering. Other KKR BZ integration methods are the so-called special directions methods.[10,16,17] They consist in decomposing the integral over the irreducible BZ segment into a weighted sum of line integrals, each line originating from the BZ center. Such methods work well for cubic lattices, whose irreducible segments are reasonably well sampled by this line grid. For lower symmetry integration domains, however, the special direction methods give less uniform samplings. This circum-

stance, as we shall see in the following, might lead to systematic integration errors.

The BZ integration presents additional problems when dealing with metals. As Blöchl *et al.*.[13] pointed out, the sampling of the Fermi surfaces is, in this case, crucial. As we shall discuss in Sec. III, for the KKR method not only the Fermi surface but also the other constant energy surfaces have to be accurately sampled.

By this paper we wish to describe the solutions we have found for the above major problems. In Sec. II we illustrate ideas to take advantage of the convergence properties of Ewald's series in order to optimize the structure constants calculation. In Sec. III we describe a BZ integration method that uses adaptive grids and we minimize the computational effort in order to reach a desired accuracy. In the same section we also describe the problems encountered in using this variable grid method in connection with the solution of the CPA equations and compare its performances with those of other currently employed techniques. All the algorithms described in Secs. II and III have been designed in order to minimize the computational work required to achieve arbitrary *input* accuracies. In Sec. IV, we discuss briefly other improvements and some features of the KKR-CPA code we implemented by applying the algorithms of Secs. II and III. This includes an integration scheme for finite temperature Green's functions. Finally, in order to illustrate the capability of the algorithms, we present in Sec. V calculations of the density of states (DOS) for pure Cu, in a number of different geometries, and for a $Cu_{0.75}Pt_{0.25}$ random alloy. We also present *ab initio* calculations for hcp and fcc Ti.

II. OPTIMIZATION OF KKR STRUCTURE CONSTANTS EVALUATION

Within the KKR method[1,2] the band structure is determined in terms of the reciprocal space poles of the scattering path operator, τ,

$$\tau(\vec{k},p)=[t^{-1}(p)-G^0(\vec{k},p)]^{-1}. \tag{1}$$

In Eq. (1), $\vec{k}$ is a reciprocal space vector and p is related to the energy E and to the speed of the light in the vacuum, c, by

$$p=\sqrt{E(1+E/c^2)}. \tag{2}$$

The lattice Fourier transform of the empty lattice propagator, $G^0(\vec{k},p)$, is conveniently written, in the angular momentum representation, in terms of the KKR structure constants, $D_{\ell,m}$[6,7], as

$$G^0_{\ell,j,m,\ell',j',m'}(\vec{k},p)=4\pi i^{\ell-\ell'} \times \sum_{\ell'',m''} C^{\ell'',m''}_{\ell,j,m\ell',j',m'} D_{\ell'',m''}(\vec{k},p), \tag{3}$$

where

$$D_{\ell,m}(\vec{k},p)=-p\sum_{\vec{r}\neq 0} e^{i\vec{k}\cdot\vec{r}} i^{-\ell+1} h^+_\ell(pr) Y^*_{\ell,m}(\vec{r}) - i\frac{p}{\sqrt{4\pi}}\delta_{\ell,0}\delta_{m,0}. \tag{4}$$

The set (ℓ,j,m) represents the orbital, total, and azimuthal quantum numbers. The coefficients $C^{\ell'',m''}_{\ell,j,m\ell',j',m'}$ are linear transformations of Gaunt numbers by Clebsh-Gordan coefficients.[18] Due to the Gaunt numbers properties,[19] m'' can only take integer values in Eq. (3), thus, only one $D_{\ell,m}$ set can be used for both relativistic and nonrelativistic calculations. The switch to the last case is straightforward: the coefficients $C^{\ell'',m''}_{\ell,j,m\ell',j',m'}$ coincide with the Gaunt numbers and $p=\sqrt{E}$. In Eq. (4), $\vec{r}$ indicates the Bravais lattice site coordinates and h^+_ℓ and $Y_{\ell,m}$ are spherical Hänkel functions and spherical harmonics. Equations (3) and (4) refer, for the sake of simplicity, to the case of one atom per unit cell lattice. The generalization to ''complex lattices'' follows straightforwardly the lines of Ref. 6 and affects the following discussion only by minor modifications. All the formulas we are going to present hold for complex energies with $\mathrm{Im}\{E\}\geqslant 0$.

Unfortunately, the structure constants evaluation by Eq. (4) could require a lot of terms. Thus, it is convenient to apply the famous Ewald's Θ transform[8] and rewrite Eq. (4) as the sum of the following three series:[6,7]

$$D_{\ell,m}(\vec{k},p)=D^{(1)}_{\ell,m}(\vec{k},p)+D^{(2)}_{\ell,m}(\vec{k},p)+D^{(3)}_{\ell,m}(p), \tag{5}$$

$$D^{(1)}_{\ell,m}(\vec{k},p)=-\frac{4\pi}{v_c}p^{-\ell}e^{p^2/\eta}\sum_{\vec{g}}\frac{|\vec{g}+\vec{k}|^\ell e^{-|\vec{g}+\vec{k}|^2/\eta}}{|\vec{g}+\vec{k}|^2-p^2} \times Y^*_{\ell,m}(\vec{g}+\vec{k}), \tag{6}$$

$$D^{(2)}_{\ell,m}(\vec{k},p)=-\frac{2}{\pi^{1/2}}(2i)^\ell p^{-\ell}\sum_{\vec{r}\neq 0} r^\ell e^{i\vec{k}\cdot\vec{r}} Y^*_{\ell,m}(\vec{r}) \times \int_{\sqrt{\eta}/2}^{\infty} d\xi \xi^{2\ell}\exp[-\xi^2 r^2+p^2/4\xi^2], \tag{7}$$

$$D^{(3)}_{\ell,m}(p)=-\frac{\eta^{1/2}}{2\pi}\sum_{s=0}^{\infty}\frac{(p^2/\eta)^s}{s!(2s-1)}\delta_{\ell,0}\delta_{m,0}, \tag{8}$$

where $\vec{g}$ are the reciprocal lattice vectors, and η is the Ewald parameter. As it is well known,[6,7] the choice of η greatly affects the convergence properties of the series: small η values cause the $\vec{k}$-space series in Eq. (6) to converge rapidly and the $\vec{r}$-space series in Eq. (7) to converge slowly, while the opposite happens for large η values. Furthermore, the lowest acceptable value of η is, in practice, fixed by the hypergeometric series in Eq. (8), whose numerical evaluation is hard for $p^2/\eta\gg 1$. For energy ranges of practical interest, it is better to avoid $\eta<0.1$.

Due to the above convergence properties of Eqs. (6)–(8), one may ask what is the η value that produces the structure constant, precise up to the given accuracy, Δ, *and* minimizes the computing time. As a matter of fact, such η_{opt} depends on the energy and the lattice geometry, the last dependence being crucial in the optimization of the computing time. In the past the best choices of η have been found by trials for

various lattices.[7] Such empirical searches are not efficient if one is interested in treating on equal footing many different lattices. However, the problem can be assessed in a very general way, as we are going to see.

First of all, let us say that, for a given energy, the structure constants have to be calculated at N_1 reciprocal space points. Of course, it is convenient to evaluate once for each energy and store the $\vec{k}$ independent parts in Eqs. (7) and (4). Now, if t_1 and t_2 are the computing times necessary for the computation of each term in the series (6) and (7), the total computing time results,

$$T=\frac{R^3}{v_c}t_2+\frac{N_1 G^3}{(8\pi^3/v_c)}t_1, \tag{9}$$

where v_c is the unit cell volume and R^3/v_c and $G^3/(8\pi^3/v_c)$ are the numbers of terms included in the series (6) and (7) that, thus, have been truncated including only the contributions with $|\vec{r}|\leqslant R$ and $|\vec{k}|\leqslant G$. Our goal here is to minimize T and achieve the input accuracy. We notice that the $\vec{k}$ dependencies of the truncation errors in Eqs. (6) and (7) are reasonably weak. In fact, the quasimomentum enters in Eq. (7) only through a phase factor, while $|\vec{k}|\ll|\vec{g}|$ is certainly satisfied for the contributions not included in the sum of Eq. (6). Thus, for the moment, we consider the truncation errors at $\vec{k}=0$, while at the end of this section we shall come back to discuss their $\vec{k}$ dependence in more detail. Furthermore, we notice that such errors, $\mathfrak{R}_\ell^{(1)}(p^2,G,\eta)$ and $\mathfrak{R}_\ell^{(2)}(p^2,R,\eta)$, do not depend on m. Thus we can write

$$\mathfrak{R}_\ell^{(1)}(p^2,G,\eta)\cong\frac{4\pi}{v_c}\eta^{-\ell/2}\phi_\ell(p^2/\eta)\sum_{|g|>G}\frac{g^\ell e^{-g^2/\eta}}{g^2-|p^2|}, \tag{10}$$

$$\mathfrak{R}_\ell^{(2)}(p^2,R,\eta)=\frac{2^{\ell+1}}{\pi^{1/2}}\eta^{-\ell/2}e^{-\mathrm{Re}[p^2/\eta]}\phi_\ell(p^2/\eta)\times\sum_{|\vec{r}|>R}r^\ell\int_{\sqrt{\eta}/2}^{\infty}dx x^{2\ell}\exp[-x^2r^2+p^2/4x^2], \tag{11}$$

where $\phi_\ell(x)=e^{\mathrm{Re}[x]}|x|^{-\ell/2}$. By taking the continuum limit of Eqs. (10) and (11), assuming that

$$G^2\gg p^2, \tag{12}$$

$$R^2\eta/4\gg 1, \tag{13}$$

and using an integral representation of the incomplete gamma function,[20] we find

$$\mathfrak{R}_\ell^{(1)}(p^2,G,\eta)\leqslant\frac{1}{\pi}\phi_\ell(p^2/\eta)\eta^{1/2}\frac{G^2}{G^2-p^2}\Gamma\left(\frac{\ell+1}{2},\frac{G^2}{\eta}\right) \tag{14}$$

and

$$\mathfrak{R}_\ell^{(2)}(p^2,R,\eta)\leqslant\frac{4\pi^{1/2}2^\ell}{v_c}\eta^{-\ell/2}\phi_\ell(p^2/\eta)\times\int_R^\infty drr^{-\ell+1}\Gamma\left(\frac{\ell+1}{2},\frac{r^2\eta}{4}\right). \tag{15}$$

Moreover, we can use the asymptotic expansion of the incomplete gamma function in Eq. (15) and obtain

$$\mathfrak{R}_\ell^{(2)}(p^2,R,\eta)\leqslant\frac{8\pi^{1/2}}{v_c}\phi_\ell(p^2/\eta)\eta^{-1}\Gamma\left(\frac{\ell+1}{2},\frac{\eta R^2}{4}\right). \tag{16}$$

As is apparent from Eqs. (14) and (16), the gamma functions dominate the decay of the errors with the truncation radii, while the energy dependencies appear only marginal. Therefore, we can have the truncation errors of both series as close as possible, simply by equating the arguments of the gamma functions, say,

$$\eta R^2/4=G^2/\eta=x. \tag{17}$$

The positive definite quantity x, as we are going to see, turns out simply related to Δ.

At this point, η_{opt} can be obtained by minimizing the expression for the total computing time, Eq. (9), where R and G are given in terms of x and η through Eq. (17). In this way we find

$$\eta_{\mathrm{opt}}=\frac{4\pi}{v_c^{2/3}}\left(\frac{t_2}{N_1t_1}\right)^{1/3}, \tag{18}$$

and, accordingly, the optimal truncation radii,

$$G_{\mathrm{opt}}=\sqrt{x\,\eta_{\mathrm{opt}}}, \tag{19}$$

$$R_{\mathrm{opt}}=2\sqrt{x/\eta_{\mathrm{opt}}}, \tag{20}$$

and the total truncation error as a function of x and of the dimensionless energy $\epsilon=p^2/\eta_{\mathrm{opt}}$,

$$\mathfrak{R}_{\ell,\mathrm{opt}}(p^2,x)=\mathfrak{R}_\ell^{(1)}(p^2,x,\eta_{\mathrm{opt}})+\mathfrak{R}_\ell^{(2)}(p^2,x,\eta_{\mathrm{opt}})\cong\frac{2\phi_\ell(\epsilon)}{v_c^{1/3}\pi^{1/2}(t_2/N_1t_1)^{1/3}}\left(1+\frac{x(t_2/N_1t_1)^{1/2}}{x-|\epsilon|}\right)\times\Gamma\left(\frac{\ell+1}{2},x\right). \tag{21}$$

In order to determine the quantity x defined in Eq. (21), we have simply to ensure that the inequalities

$$\mathfrak{R}_{\ell,\mathrm{opt}}(p^2,x)\leqslant\Delta \tag{22}$$

are satisfied. This is easily accomplished since, in the asymptotic regime, the truncation error decreases monotonically as a function of x.

Remarkably, our method gives a weak energy dependence for η_{opt}, at least for the energy ranges of practical interest. Moreover, when applied to a fcc lattice with $N_1=1$, $t_1=t_2$, we get essentially the same value suggested by Davis.[7] However, in our case, no test runs are needed to decide the Ewald parameter best value for the lattice and the energy considered: once x is determined, it is sufficient to establish the order of magnitude of N_1 and the machine dependent ratio t_2/t_1. Our best choice on IBM Power Risc workstations is

$t_2/t_1 N_1 \sim 10^{-2}$, where we include N_1 (~ 1000) as appropriate to our BZ integration method (see Sec. III).

At this point we have to come back to the $\vec{k}$ dependence of the truncation errors. At nonzero wave vectors, the condition (12) should be replaced by

$$|\vec{G}+\vec{k}|^2 \gg p^2. \tag{23}$$

In order to ensure that this is satisfied for all the BZ points, it is sufficient to increase $G_{\rm opt}$, as given by Eq. (19), by the maximum length of the BZ. Analogously, when complex lattices are considered, Eq. (7) has to be satisfied for each sublattice, and, accordingly, $R_{\rm opt}$, as given by Eq. (20), must be incremented by the length of the largest translation vector in the unit cell.

We have used the same kind of error analysis in order to compare our algorithm with the direct summation of Eq. (4). In the last case, the decay of the error is dominated by the Hänkel function in Eq. (4), and, for a given accuracy, Ewald's method turns out to be faster in most of the complex energy upper half plane, while the direct summation is preferable only close to the real axis well below the energy zero or at a very high imaginary part of the energy. To summarize, Ewald's method appears quite generally convenient for constant energy KKR calculations and our algorithm can be applied to any lattice ensuring the achievement of an arbitrary small accuracy.

III. METHODS FOR BRILLOUIN ZONE INTEGRATION

As quoted in the Introduction, the BZ integration of the KKR scattering path matrix elements is a hard numerical problem, due to the pole structure of the integrands, which diverge whenever the KKR determinant goes to zero.[1] Therefore, an accurate integral requires a high density of grid points *only* close to the poles. As a consequence, $\vec{k}$-space uniform grids methods, as special points or tetrahedron methods,[14,13] are not efficient. In the early times of KKR-CPA calculations,[9,10] in fact, the so-called Zoomin procedure was used, in connection with the special direction methods.[10,16,17] These methods, briefly, consist in transforming the volume integral into a weighted sum of line integrals. Each line originates from the center of the BZ and intersects its boundaries defining an elemental prism. The corresponding weights can be chosen, in different schemes, as the volumes of these prisms (Stocks' prism method,[10]) through a convenient cubic harmonics expansion[16] or in combination with a two-dimensional Gaussian quadrature.[17]

In the Zoomin method, for each line, the integrands are evaluated at first on a reasonably coarse grid, and afterwards new points are inserted whenever the variations of the integrand are larger than a prescribed amount and the integrals are evaluated by ordinary quadrature variable grid methods. Later on, a method has been implemented,[11] based on a rational function local fit of the integrands that does not require the Zoomin procedure. A slightly different version of this will be described in Sec. III B.

The special direction methods work reasonably well for cubic lattices, because their irreducible segments are sampled almost uniformly by the radial directions grids. These techniques, however, present a few inconveniences. In the first place, the region around the Γ point is sampled much more densely than the BZ borders. Thus, it could happen, particularly in the case of Van Hove singularities at the BZ boundaries, that a large number of directions must be used. This inconvenience is worsened in the case of low symmetry Bravais lattices, whose irreducible segment shape is often less similar to a spherical fuse than for cubic lattices. Moreover, it is difficult to decide the ideal size of the spacing between the points in the initial grid. This, in fact, should be neither too wide, in order to find all the structures of the integrand, nor too narrow, in order to reduce the amount of calculation. Last, but not least, there is no simple way to estimate the integration errors, which, because of the geometrical structure of the method, are not simple functions of the number of directions and, certainly, depend on the topologies of the constant energy surfaces.[21,13]

A. An adaptive quadrature algorithm

The above discussion suggests that the KKR integral could be performed more effectively by adaptive quadrature methods.[22] These allow the use of variable integration grids and enable performing integrals precise up to a fixed accuracy. In our algorithm, the BZ quadrature is carried out as a sequence of three line integrals, i.e.,

$$I=\int_{c_1}^{c_2} dc \int_{b_1(c)}^{b_2(c)} db \int_{a_1(b,c)}^{a_2(b,c)} f(a,b,c)\,da. \tag{24}$$

Here a, b, and c are curvilinear coordinates along three linearly independent directions, appropriate to the lattice geometry at hand (for instance, the three primitive translation vectors of the reciprocal lattice or any appropriate coordinates set). The integration domain is the irreducible segment of the BZ. Thus, the functions $b_{1,2}(c)$ and $a_{1,2}(b,c)$ and the limits $c_{1,2}$ have to be determined for each Bravais lattice. For most of the lattices such functions present cusps in connection with the frontier of the integration domain. In this case it is convenient to break the integration intervals into segments limited by the above singularities.

In order to evaluate each line integral, we proceed as follows. Given an integration tolerance, ϵ, our algorithm consists in the iteration of the following four steps.

Step I. We mark three points on the integration interval, call them the first, the last, and the middle point, x_f, x_l, and $x_m=(x_f+x_l)/2$, and evaluate the integrand at each point.

Step II. We evaluate the integral, over the current interval, both by Simpson's and the trapezoidal rules, as

$$I_s=\frac{1}{6}(x_l-x_f)[f(x_f)+4f(x_m)+f(x_l)]+O[(x_l-x_f)^5], \tag{25}$$

$$I_t=\frac{1}{2}(x_l-x_f)\left[\frac{1}{2}f(x_f)+f(x_m)+\frac{1}{2}f(x_l)\right]+O[(x_l-x_f)^3]. \tag{26}$$

Then, if the inequality

$$r=\frac{|I_s-I_t|}{|I_s|}\leqslant\epsilon \tag{27}$$

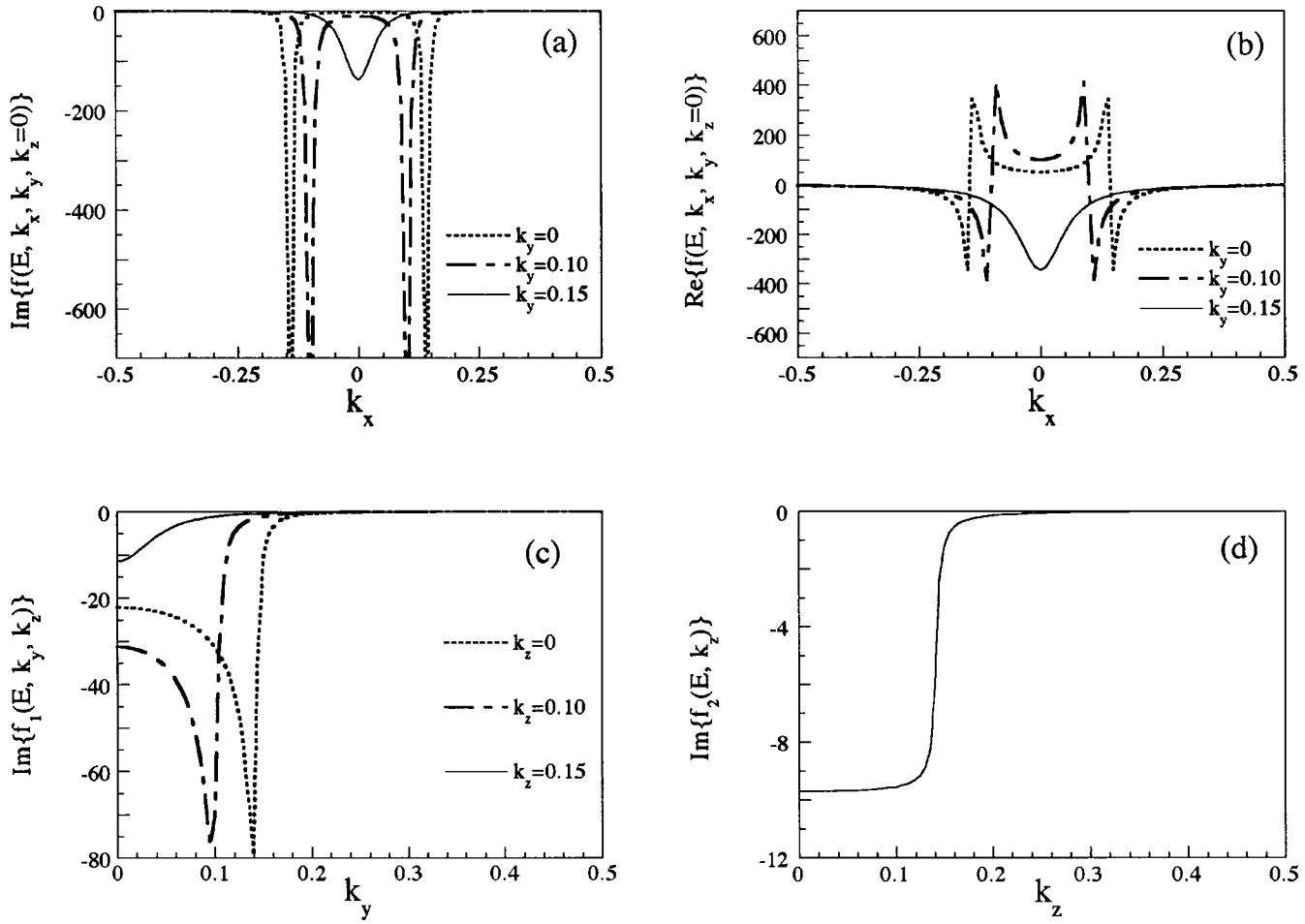

FIG. 1. Free electron Green's function integration [see Eqs. (35), (37) and (38)] for a simple cubic lattice at $E=0.2+i0.001$. (a) and (b) Imaginary and real parts of f vs k_x, at the indicated values of k_y and k_z. (c) Imaginary part of f_1 vs k_y, at the indicated values of k_z. (d) Imaginary part of f_2 vs k_z.

is satisfied, I_s is assumed correct, the estimated integration error over the current interval is set to $r|I_s|(x_l-x_f)^4$, and we jump to step IV.

Step III. Inequality (27) is not verified, i.e., the integrand is not smooth enough to achieve the accuracy ϵ. Then we have to insert more points into the grid. Rather than to proceed as in the Romberg method, namely by halving the step throughout, we forget, for the moment, the second half interval, and insert a single new point in the middle of the first half. Then we ''shift down'' the current three point labels, save temporarily the function value and the grid point not used for the time being (i.e., the former last point value), and go back to step II. All this is iterated until the inequality (27) is verified for the current interval.

Step IV. The result for the current interval is accumulated and we proceed to integrate over the rest of the line, by ''shifting up'' the x_f, x_l, and x_m definitions. In order to save memory, it is convenient to discard the function and the grid point, which are no longer necessary (i.e., the first point of the last cycle). Then we go back to step II or exit if the integral is completed.

The iterative halving (step III) is designed to insert as many points as needed to achieve the prescribed accuracy ϵ.

In order to carry on volume integrals, the above step procedure has been coded as cascade routines. Since we integrate matrices, it is convenient to check the inequality (27) for their traces. This method provides an elegant way to zoom in where the integrand changes abruptly, while only a few points are used where it is smooth. For instance, as a consequence of its adaptive nature, our method automatically uses few points at energies high in the complex plane and more points close to the real axis.

In order to discuss the applicability of the above adaptive method, we have used the simple free-electron band model. For low energies the relevant elements of the scattering path matrix, in this model, are proportional to

$$f(E,\vec{k})=\frac{1}{E-k^2} \tag{28}$$

and the corresponding DOS is given by

$$n(E)\propto -\frac{1}{\pi}\mathrm{Im}\left\{\int_{\mathrm{BZ}} d\vec{k} f(E,\vec{k})\right\}. \tag{29}$$

At $\mathrm{Im}\{E\}=0$, Eq. (28) consists in a superposition of δ-like contributions at $k^2=E$. Of course, the numerical integration is possible only when $\mathrm{Im}\{E\}>0$ and the δ contributions are broadened into Lorentzians [see Figs. 1(a) and 1(b), where

we have plotted $f(E,\vec{k})$ for a simple cubic lattice]. The numerical integration of $f(E,\vec{k})$ along a line, at small Im$\{E\}$, is difficult since catching the sharp peaks plotted in Figs. 1(a) and 1(b) could require a huge number of points. However, in this case, the tangentlike behavior of the real part of the integrand allows our adaptive algorithm to insert points only in the region of sharp variations. This leads to a good accuracy down to quite low values of Im$\{E\}$. However, close to the real axis, the method might fail. In this case, as we shall discuss in the next subsection, the rational fit method usually leads to better results. In any case, once

$$f_1(E,k_y,k_z)=\int dk_x f(E,k_x,k_y,k_z) \tag{30}$$

is obtained, the adaptive method is accurate and efficient. In fact, by looking at the features of Fig. 1(c), we easily realize that our algorithm is always able to locate the jumps of the integrand and insert only the necessary points. Analogously, the next integration,

$$f_2(E,k_z)=\int dk_y f_1(E,k_y,k_z), \tag{31}$$

is performed with very few points located at the function jump [see Fig. 1(d)].

From the above analysis, we conclude that this method is well tuned for integrating KKR matrices. Of course, for energies close to the real axis, the number of points required for the innermost integration could be quite large. To avoid such a problem and the risk of losing structures, a different algorithm could be preferable. In the next subsection we shall discuss a rational fit quadrature method that is able to deal with these difficulties.

B. Rational functions fit quadrature and hybrid method

The scattering path matrix is evaluated as the inverse of the KKR matrix [see Eq. (1)]. Then we can write for the innermost integration:[11]

$$I_{L,L'}(p^2,b,c)=\int_{a_1}^{a_2} dx[t^{-1}(p^2)-G^0(x,b,c,p^2)]^{-1}_{L,L'}$$

$$=\int_{a_1}^{a_2} dx \frac{M_{L,L'}(x)}{D(x)}, \tag{32}$$

where $M_{L,L'}(x)$ is the cofactor of the KKR matrix and $D(x)$ its determinant, both evaluated at the x_i points of a grid along the current direction. Both $M_{L,L'}(x)$ and $D(x)$ are smooth functions of x, the peaks of the integrands arising when the determinant becomes small. Then, one can fit both cofactor and determinant in Eq. (32) by two nth degree polynomials at each $n+1$ adjacent point of the grid. Then, after a study of the roots of the denominator, the integral can be performed analytically over each interval.

This elegant trick[11] can be checked against analytic functions, and does not require dense grids along each line. It can be used, then, in order to deal with the a integration of Eq. (24), while both b and c integrations can be efficiently performed by the adaptive method described in Sec. III A. The resulting hybrid algorithm, even near the real energy axis, does not present the occasional inconveniences of the triple adaptive quadrature and is frequently more efficient at any energy. In effect, this method deals directly with the poles of the integrands along the line and allows a sort of semianalytical treatment of the integral in a neighborhood of the poles themselves. Moreover, it produces a grid of lines (in this case) more dense where needed, i.e., where there are states. To put it in another way, this hybrid method can be thought of as a prism method with an adaptive direction grid.

The small inconvenience of this procedure is that the integration error estimate now refers only to the outermost integrations, the rational fit integration being assumed exact. The last, of course, is precise only if the step used in the line integration is appropriately sized. The optimum value of this step, Δk, could be found by trials. Our experience suggests that a good choice for Δk should depend on the imaginary part of the energy and on the lattice geometry as well. In this paper we have taken $\Delta k \propto a_{\max}(v_c N_c)^{(-1/3)}\mathrm{Im}\{E\}$, where $a_{\max}$ is the maximum length in the Brillouin zone along the a-integration direction.

We would like to illustrate by an example some features of the hybrid method in comparison with other BZ integration methods. Let us imagine that, for a given crystal, we have a Van Hove singularity at the real energy E_1 at the point $\vec{k}_1$. For instance, let us suppose that the Van Hove singularity is due to a band minimum. Then for $E>E_1$ there is an electron pocket. In a neighborhood of E_1, the pocket linear dimension is proportional to $\Delta=(E-E_1)^{1/2}\Theta(E-E_1)$, according to the theory of the electronic topological transitions.[21] A uniform mesh of $\vec{k}$ points, as for instance in the case of the tetrahedron method, fails to account for this pocket if the mean spacing between the grid points is larger than Δ. The special direction methods would be able to catch the pocket if $|\vec{k}_1|$ is small (in this case the relevant spacing is $|\vec{k}_1|^2\Delta\omega$, where $\Delta\omega\propto 1/N_{\mathrm{dir}}^2$), but they could easily miss pockets close to the BZ borders. It is easy to realize that the tetrahedron method requires $N\propto\Delta^{-3}$ points to solve such a structure, while the special directions method needs $N_{\mathrm{dir}}\propto|\vec{k}_1|/\Delta^{1/2}$ directions or $N=nN_{\mathrm{dir}}$ points, if n is the mean number of points per direction. Of course, n has to be large enough to ensure a correct line integration. Our hybrid method is *always* able to resolve the above structure by inserting very few lines where necessary, provided the above condition on n is satisfied. However, far from the real energy axis, the additional smearing of the Green's functions reduces the above inconveniences. Then the error on the total energy, normally calculated as an integral over a complex contour, is essentially the error of the BZ integration at the Fermi energy and, then, is relevant only for metals.

As a further consequence of the above arguments, for energy dependent quantities, uniform mesh methods could give errors that vary smoothly with the energy, while the errors of the hybrid method are essentially random.

C. Semianalytical tests

We have implemented the hybrid method for the BZ integration. In order to study its capabilities, we have tried to integrate the function of Eq. (28) over the BZ of a simple cubic lattice. This function can be integrated analytically as a

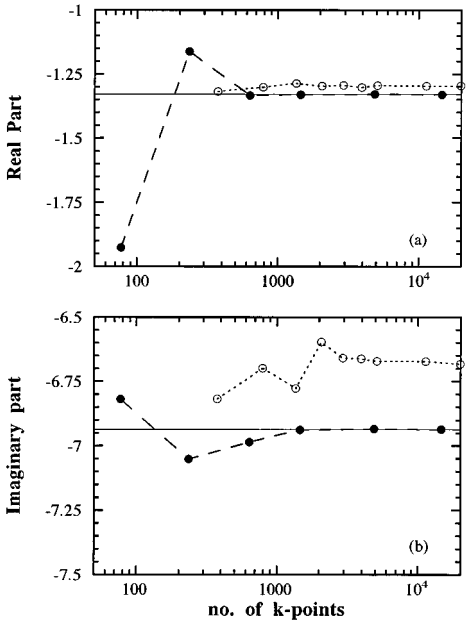

FIG. 2. Semianalytic test of the hybrid method I (see text). The integrand is the free electron model Green's function [Eq. (35)] at $E=0.2+i0.05$. The abscissa shows the number of the function evaluation. Full circles, hybrid method; empty circles, prism method; horizontal lines, exact results. (a) Real part of the integral; (b) imaginary part of the integral.

function of k_x and then numerically, by standard mathematical software up to a very high precision, for the simple cubic lattice. However, its full numerical integration in the irreducible BZ segment is very hard, as it can be seen from Fig. 1.

In Fig. 2 we show the results obtained by our method and the prism method, vs the number of function evaluations

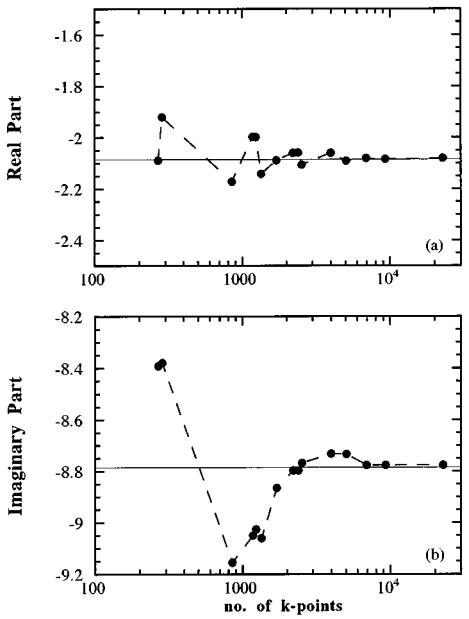

FIG. 3. Semianalytic test of the hybrid method II (see text). Long dashed lines with full circles, hybrid method; horizontal lines, exact results. (a) Real part of the integral; (b) imaginary part of the integral. The energy is $E=0.2+i0.001$.

required, at $E=0.2+i0.05$. In the calculations with the prism method we have varied the number of radial directions, keeping fixed the density of points along each line, and we have calculated each line integral with the rational fit method described in the preceding subsection [apart from a factor x^2 in Eq. (32)]. The real and imaginary parts of the BZ integral are displayed in Figs. 2(a) and 2(b), respectively, while the horizontal lines represent the exact results. As the reader can see, even with a large number of grid points, the directions method does not appear converging toward the exact results, revealing the presence of systematic errors. It is worth mentioning here that, among the cubic systems, the simple cubic lattice geometry enhances the inconveniences of the special directions method, namely the nonuniformity of its sampling. Our method, instead, is able to give an accurate result using a relatively small number of points.

In Fig. 3 we show the integral of the same function vs the number of points, at $E=0.2+i0.001$, where the integration is expected to be much harder. Again the reader can see that our adaptive method works accurately, using more points than before, as expected, due to the pathology of the integrand. We wish to remark that for the calculations shown in Figs. 2 and 3, the errors of our method are of the order of magnitude of the input integration tolerance ϵ.

D. Problems connected with KKR-CPA

In order to discuss the applicability of our BZ integration scheme in connection with the CPA, we briefly recall, dropping the angular momentum indices and the energy dependencies, the set of KKR-CPA equations:[9,23]

$$\tau_c^{00}=\frac{v_c}{8\pi_3}\int [t_c^{-1}-G^0(\vec{k})]^{-1}d\vec{k}, \tag{33}$$

$$\sum_\alpha c_\alpha \tau_\alpha^{00}=\tau_c^{00}, \tag{34}$$

$$\tau_\alpha^{00}=D_\alpha \tau_c^{00}, \tag{35}$$

$$D_\alpha=[1+\tau_c^{00}(t_\alpha^{-1}-t_c^{-1})]^{-1}, \tag{36}$$

where c_α is the concentration, t_α the single site t matrix of the α atomic species, t_c and τ_c^{00} are the effective medium single site t matrix and the central site scattering path matrix, and D_α is the so-called CPA projector, which allows us to extract the conditional averages (the α atomic species at the central site) of the scattering path matrix, τ_α^{00}.

KKR-CPA equations are solved by iteration, until stationarity for t_c is achieved within a given tolerance, ϵ_{CPA}. This procedure, of course, requires one BZ integration for each cycle. The errors in the BZ integration affect the solution for t_c. Using fixed $\vec{k}$ points grids, when close to convergence, the integration errors cancel out since they appear on both sides of the CPA condition, Eq. (34). If the integration is carried on by an adaptive method, although both are smaller than the integration tolerance ϵ, the errors in two successive cycles cannot cancel out precisely in the CPA condition. As a consequence, the iterative solution of the CPA equation set will be affected by numerical disturbances, and, occasionally, could fail when $\epsilon \gg \epsilon_{\mathrm{CPA}}$. However, setting $\epsilon=\epsilon_{\mathrm{CPA}}$ it

TABLE I. DOS and number of function evaluations, N_1, at $E=0.4+i0.02$ for a Cu site potential (ASA), obtained by the hybrid method (see Sec. III B) with integration tolerance $\epsilon=10^{-4}$. The calculations refer to fcc, bcc, and sc lattices and to several lattices, whose parameters have been chosen to obtain coincidence with the three cubic systems. Equivalent systems are listed in the same row. In all the systems the atomic volume has been kept fixed to 75.528 (Bohr^3). The DOS values are in spin/Ry. Abbreviations are as follows: fcc, face centered cubic; fct, face centered tetragonal; fco, face centered orthorhombic; bcc, body centered cubic; bct, body centered tetragonal; bco, body centered orthorhombic; sc, simple cubic; st, simple tetragonal; so, simple orthorhombic; sm, simple monoclinic; trig, trigonal; tric, triclinic; $L1_2$, Cu_3Au; $L1_0$, CuAu; $B2$, CsCl; $D0_3$, Fe_3Al; $B1$, NaCl.

Lattice	fcc	fct	fco	trig	$L1_2$	$L1_0$	$L1_1$
DOS	32.748	32.714	32.733	32.742	32.714	32.749	32.737
N_1	2277	3047	5846	3258	1149	1853	3707
Lattice	bcc	bct	bco	trig	tric	$B2$	$D0_3$
DOS	35.339	35.341	35.314	35.317	35.352	35.337	35.337
N_1	1537	2720	5809	2643	11921	1166	2270
Lattice	sc	st	so	trig	sm	tric	$B1$
DOS	31.573	31.542	31.524	31.578	31.524	31.515	31.590
N_1	1792	2898	3707	3506	7367	14326	2999

is not at all a way out. In fact, in standard calculations ϵ_{CPA} is usually set to quite small values ($\sim 10^{-6}$). This is due to the need to ensure cancellations between the coherent and incoherent parts in the Bloch spectral functions.[23] Unfortunately, such a small integration tolerance would require a huge number of evaluations, making the calculation prohibitive, but is not really necessary when calculating site diagonal observables, such as density of states, charge densities, or electronic total energy. Then, a fair compromise could be achieved by fixing $\epsilon=10^2\epsilon_{\mathrm{CPA}}$.

IV. TEST CALCULATIONS

We have developed a KKR-CPA code, in which we have implemented the algorithms described in the former sections. Our starting point has been the well optimized code of Ref. 5 and a structure constants code kindly shared by Wang and Stocks. We have developed two versions: a ''serial'' and a parallel version based on the PVM package.[24] Our code can work for nonrelativistic, scalar relativistic, or fully relativistic problems, for what concerns the valence states, and deals with the core states either fully or nonrelativistically. It can be used for pure metals, intermetallic compounds, random alloys (CPA), many sublattice random alloys, and for zero as well as for finite temperature calculations. All the Bravais lattices and most common complex lattices have been implemented. In order to ensure generality, we have preferred the complex spherical harmonics (and the spin angular harmonics for the fully relativistic case) as the angular momentum basis set, rather than lattice point group symmetrized sets. The potential treatment is either by the nonoverlapping muffin-tin or atomic sphere approximation (ASA). A full potential treatment and a spin polarized version are in development. The total energy calculations and the potential reconstruction follow the lines of Ref. 25.

We have singled out the DOS as the appropriate observable to check, at the same time, our structure constants and BZ integration algorithms. In all the test calculations we are going to discuss, we have truncated the angular momentum expansions to $\ell\leqslant 3$. In Table I we show the DOS calculated at the indicated energy for Cu, in the ASA approximation, and for several lattices. The lattice parameters and the atom positions in the unit cell have been tuned in such a way that all the structures are coincident with one of the three cubic lattices. The BZ integral is carried on by our hybrid method. The step for the rational fit integration has been let to vary in the range 0.03–0.1, according to the discussion of Sec. III B. The integration accuracy has been fixed to the very tight value $\epsilon=10^{-4}$. As the reader can see, the results agree within absolutely tolerable fluctuations, all of the order of

TABLE II. Comparison between DOS calculated by different integration methods. Our hybrid method results (labeled by HM), calculated with $\epsilon=10^{-3}$, are compared with Stocks' prism method (Ref. 10), with 36, 136, and 528 directions, labeled respectively, as P36, P136, and P528. Mean values and standard deviations for various geometrically equivalent structures are obtained from the HM calculations with $\epsilon=10^{-4}$ displayed in Table I. The energy, the potentials, the units, and other symbols are the same as in Table I.

Lattice			fcc				$L1_2$		
method	HM	P36	P136	P528	HM	P36	P136	P528	Mean value
DOS	32.829	32.812	32.751	32.740	32.985	32.701	32.711	32.715	32.734 ± 0.015
N_1	682	695	2624	10194	299	1030	3895	15129	
Lattice			bcc				$B2$		
method	HM	P36	P136	P528	HM	P36	P136	P528	Mean value
DOS	35.371	35.403	35.367	35.349	35.329	35.360	35.336	35.331	35.334 ± 0.014
N_1	470	705	2662	10138	299	859	3248	12614	
Lattice			sc				$B1$		
method	HM	P36	P136	P528	HM	P36	P136	P528	Mean value
DOS	31.212	31.564	31.553	31.551	31.594	31.468	31.432	31.428	31.549 ± 0.030
N_1	350	724	2733	10621	896	822	3109	12805	

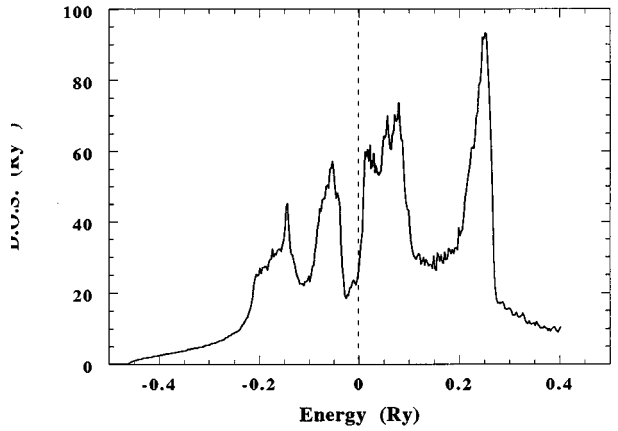

FIG. 4. The density of states of hcp Ti. The lattice parameter, $a = 5.522$ a.u., is the same as in Ref. 26. The calculation is nonrelativistic for the valence states and fully relativistic for the core states.

magnitude of the integration tolerance.

Actually, this is quite a severe test, because the integration domains, the symmetry group rotations, etc., are totally different for the various coincident systems. In fact, the bands of various equivalent lattices are folded in different ways, according to the lattice symmetry groups. We observe that the number of points used varies much less than linearly with the volumes of the irreducible segments. This is, indeed, a success of our integration method.

In Table II the results for the DOS obtained by the hybrid method with $\epsilon = 10^{-3}$ are compared with those by the prism method, with 36, 136, and 528 directions. In all cases, the KKR structure constants have been evaluated according to the theory of Sec. II. In the same table the DOS mean values and standard deviations, taken from Table I, are also reported for each class of equivalent lattices. As it can be seen, the prism method requires more points than ours to achieve comparable accuracy. For low accuracy the performances of the two methods are not too different. However, the computational advantages of our method are greatly enhanced when higher accuracies ($\epsilon = 10^{-4}$) are required. That is due to the capability of the hybrid method to insert lines more densely where needed.

We have also performed the same calculations of Table I by the full adaptive method of Sec. III A. The results for the DOS are close to the ones displayed but the number of integration points are normally bigger.

A more complete test is the *ab initio* calculation for the hcp Ti, in the nonrelativistic approximation for the valence states. The lattice parameters are the same as in Ref. 26. The DOS, plotted in Fig. 4, and the Fermi level agree quite well with Ref. 26 and other published DOS's, as Fig. 1 of Ref. 27. The little noise visible in the energy regions around 0.2 Ry and above 0.3 Ry is due to the fact that the errors in our integration method are essentially random.

We have also calculated the electronic total energy of fcc Ti, which, as expected, turns out bigger than in the hcp phase by about 3 mRy per atom. This is consistent with the Ti experimental phase diagram.[28]

In Fig. 5 we report our relativistic calculation for the DOS of $Cu_{0.75}$-$Pt_{0.25}$ random alloy, as obtained by the special direction method (a), the hybrid method applied to the fcc lattice (b), and to an fct lattice coincident with the fcc (c). All calculations agree well with other published DOS's (Fig. 2 of Ref. 29). In this plot, one can see how the old method and the new one are in reasonably good agreement, notwithstanding some oscillations around $E = 0.42$ Ry, where the curve (a) differs from (b) and (c). The last two, instead, are indistinguishable. Also recalling the semianalytic tests of the former section, and on the basis of the results of Tables I and II, we think that for the DOS calculation of Fig. 5 the hybrid method proves to be more precise than the special directions method.

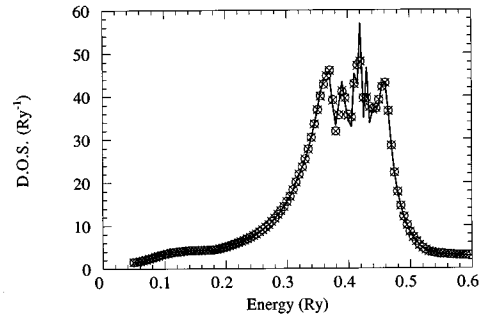

FIG. 5. The KKR-CPA density of states for $Cu_{0.75}$-$Pt_{0.25}$ random alloy. (a) Continuous line: the special direction method; (b) empty circles: hybrid method for the fcc lattice; (c) ''x'': hybrid method for the fct lattice with $c/a = 1$.

On the basis of the presented results we are confident that (i) the hybrid method is applicable to any Bravais lattice; (ii) owing to its adaptive nature, it allows precise integrals; (iii) our structure constants calculation, rotation matrices, and energy integrations are correct; and (iv) KKR-CPA calculations with calculated structure constants, applicable to any Bravais lattice, are now feasible.

V. SUMMARY

We have developed a code for LDA-KKR-CPA calculations able to deal with any Bravais lattice. We have (i) suggested an algorithm to improve the KKR structure constants calculation and (ii) designed and developed an adaptive quadrature method for BZ integration.

We have presented a test of our integration algorithm using a free electron model Green's function and calculations for various real systems. We are planning to apply this code to the calculation of electronic properties of noncubic alloys, such as In-Tl and high critical temperature superconductors.

ACKNOWLEDGMENTS

We would like to thank Y. Wang and G.M. Stocks for sharing their structure constants and MKKRCPA codes from which we started. We also thank E.S. Giuliano for discussions and his continuous encouragements. We acknowledge the facilities, scientific contacts, and discussions offered by the E.U. Ψ_k HCM Network. This work has been sponsored by MURST 60% (Italy) and INFM (Italy) funds.

[1] I. Korringa, Physica **13**, 392 (1947); W. Kohn and N. Rostoker, Phys. Rev. **4**, 1111 (1954).
[2] P. Lloyd and P.V. Smith, Adv. Phys. **21**, 69 (1972); B.L. Gyorffy, Phys. Rev. B **5**, 2382 (1972).
[3] P. Soven, Phys. Rev. **156**, 1017 (1967).
[4] See, for example, G.M. Stocks, D.M.C. Nicholson, W.A. Shelton, B.L. Gyorffy, F.J. Pinski, D.D. Johnson, J.B. Staunton, B. Ginatempo, P.E.A. Turchi, and M. Sluiter, in *Statics and Dynamics of Alloy Phase Transformations*, edited by P.E.A. Turchi and A. Gonis, Vol. 319 of NATO Advanced Study Institute Series B: Physics (Plenum Press, New York, 1994), p. 3205, and references therein.
[5] G.A. Geist, B. Ginatempo, W.A. Shelton, and G.M. Stocks, J. Supercomp. **6**, 153 (1994).
[6] F.S. Ham and B. Segall, Phys. Rev. **164**, 1786 (1961).
[7] H.L. Davis, in *Computational Methods in Band Theory*, edited by P.M. Marcus, J.F. Janak, and A.R. Williams (Plenum Press, New York, 1971), p. 183.
[8] P. Ewald, Ann. Phys. **64**, 253 (1921).
[9] G.M. Stocks, W.M. Temmerman, and B.L. Gyorffy, Phys. Rev. Lett. **41**, 339 (1978).
[10] G.M. Stocks, W.M. Temmerman, and B.L. Gyorffy, in *Electrons in Disordered Metals and at Metallic Surfaces*, edited by P. Phariseau, B.L. Gyorffy, and L. Scheire, Vol. 42 of NATO Advanced Study Institute Series B: Physics (Plenum Press, New York, 1979), p. 193; *ibid.* Vol. 41 (Plenum, New York, 1978), p. 339.
[11] F.J. Pinski and G.M. Stocks (private communications).
[12] P. Giannozzi, G. Grosso, and G.P. Pastori Parravicini, Phys. Rev. B **27**, 7553 (1983).
[13] See, for example, P. Blöchl, O. Jepsen, and O.K Andersen, Phys. Rev. B **49**, 16 223 (1994), and references therein.
[14] See, for example, S. Froyen, Phys. Rev. B **39**, 3168 (1989), and references therein.
[15] R. Zeller, in *Metallic Alloys: Experimental and Theoretical Perspectives*, edited by J.S. Faulkner and R.G. Jordan, Vol. 256 of NATO Advanced Study Institute Series E: Applied Sciences (Kluwer Academic, Dordrecht, 1994), p. 413; J.P. Dekker, A. Lodder, R. Zeller, and A.F. Tatarchenko, Solid State Commun. **97**, 1013 (1996).
[16] A. Bansil, Solid State Commun. **16**, 885 (1975).
[17] W.H. Fehlner and S.H. Vosko, Can. J. Phys. **54**, 2159 (1976).
[18] Y. Onodera and M. Okazaki, J. Phys. Soc. Jpn. **21**, 2400 (1966).
[19] See, for example, A.R. Edmonds, *Angular Momentum in Quantum Mechanics* (Princeton University Press, Princeton, 1957).
[20] I. S. Gradshtein and I.M. Ryzhik, *Table of Integrals, Series and Products* (Academic Press, San Diego, 1980).
[21] E. Bruno, B. Ginatempo, E.S. Giuliano, A.V. Ruban, and Yu.Kh. Vekilov, Phys. Rep. **249**, 353 (1994), and references therein.
[22] L.W. Johnson and R.D. Riess, *Numerical Analysis*, 2nd ed. (Addison Wesley, London, 1982).
[23] J.S. Faulkner and G.M. Stocks, Phys. Rev. B **21**, 3222 (1980).
[24] The Parallel Virtual Machine (PVM) package has been obtained by anonymous ftp from netlib@ornl.gov.
[25] D.D. Johnson, D.M. Nicholson, F.J. Pinski, B.L Gyorffy, and G.M. Stocks, Phys. Rev. Lett. **56**, 2088 (1986); D. D. Johnson, D. M. Nicholson, F. J. Pinski, B. L. Gyorffy, and G. M. Stocks, Phys. Rev. B **41**, 9701 (1990).
[26] A.M. Begley and W.M. Temmerman (unpublished).
[27] I. Bakonyi, H. Ebert, and A.I. Liechtenstein, Phys. Rev. B **48**, 7841 (1993).
[28] W.B. Pearson, *A Handbook of Lattice Spacings and Structures of Metals and Alloys* (Pergamon Press, London, 1958).
[29] B. Ginatempo, G.Y. Guo, W.M. Temmerman, J.B. Staunton, and P.J. Durham, Phys. Rev. B **42**, 2761 (1990).